metals

MDPI

Article

Demonstrating In Situ Formation of Globular Microstructure for Thixotropic Printing of EN AW-4043 Aluminum Alloy

Silvia Marola * and Maurizio Vedani

Department of Mechanical Engineering, Politecnico di Milano, Via G. La Masa 1, 20156 Milano, Italy; maurizio.vedani@polimi.it

* Correspondence: silvia.marola@polimi.it; Tel.: +39-02-23998679

Abstract

This study explores the feasibility of generating a globular microstructure in situ during the thixotropic 3D printing of the EN AW-4043 alloy, starting from a conventional cold-rolled wire. Thermodynamic simulations using Thermo-Calc software were first conducted to identify the semi-solid processing window of the alloy, based on the evolution of liquid and solid fractions as a function of temperature. Guided by these results, thermal treatments were performed on cold-rolled wires to promote the formation of a globular microstructure. A laboratory-scale printing head prototype was then designed and built to test continuous heating and deposition conditions representative of a thixotropic additive manufacturing process. The results showed that a globular microstructure could be achieved in the cold-rolled EN AW-4043 wires by heating them at 590 °C for 5 min in a static muffle furnace. A similar effect was observed when continuously heating the wire while it flowed through the heated printing head. Preliminary deposition tests confirmed the viability of this approach and demonstrated that thixotropic 3D printing of EN AW-4043 alloy is achievable without the need for pre-globular feedstock.

Keywords: thixotropic 3D printing; semi-solid metal processing; aluminum alloy; globular microstructure

Academic Editor: Golden Kumar

Received: 9 June 2025
Revised: 14 July 2025
Accepted: 16 July 2025
Published: 17 July 2025

Citation: Marola, S.; Vedani, M. Demonstrating In Situ Formation of Globular Microstructure for Thixotropic Printing of EN AW-4043 Aluminum Alloy. *Metals* **2025**, *15*, 804. https://doi.org/10.3390/met15070804

1. Introduction

Thixotropy—the rheological property exhibited by certain materials to reduce their viscosity under shear stress and recover it once the stress is removed—has been studied since the early 1920s. Over time, its definition has evolved from a purely time-dependent behavior to a broader concept, particularly following the development of semi-solid metal processing (SSP) in the 1970s [1–5].

SSP is a manufacturing technique that operates within the solid–liquid coexistence region of a metallic alloy (typically at solid fractions between 0.3 and 0.6) [2,6]. It combines the advantages of conventional casting and forging, enabling the production of complex metallic components with improved mechanical properties, reduced porosity, and enhanced dimensional precision [6]. Additionally, because the alloy is only partially melted, SSP requires lower thermal energy input than fully molten processes, resulting in greater energy efficiency, reduced mold wear, and shorter cycle times [2].

According to the literature [1,2,5,7,8], successful semi-solid processing of a metallic alloy requires selecting a composition with a wide solidification range (i.e., the interval between solidus and liquidus temperatures) and starting with a near-globular grain structure. When shear forces are applied, near-globular particles can move easily past one

another, leading to a decrease in viscosity and causing the material to behave almost like a liquid. In contrast, when shear is applied to the dendritic microstructures typically found in conventional castings, the liquid becomes trapped between the dendritic arms, restricting movement and increasing the material's viscosity. Therefore, a key requirement for SSP is a globular microstructure, in which near-spherical solid grains are dispersed in a liquid matrix. The process of converting an initially dendritic structure into this more favorable morphology is known as globularization. This transformation enhances the alloy's ability to flow under shear without fragmentation, an essential characteristic for achieving the desired thixotropic behavior [2,5,7,8].

Several methods have been developed to obtain globular feedstock for SSP. These are typically classified into two approaches: the rheo-route (hence the terms rheo-forming or rheo-casting) and the thixo-route (hence thixo-forming) [1,2]. The rheo-route involves generating a semi-solid slurry with spheroidal (non-dendritic) microstructure by vigorously stirring the melt during slow solidification, followed by transferring the slurry into a die or mold for the final shaping or solidifying it into a semi-finished product. The thixo-route, by contrast, is a two-step process that uses feedstock with a globular microstructure—typically produced via the rheo-route—which is then reheated within the semi-solid temperature range to form a slurry. This slurry is subsequently molded into the final part [1,2].

A notable variation of the thixo-route is the strain-induced melt activation (SIMA) process, which involves cold working a starting alloy billet of reduced section (typically a bar or wire), followed by reheating it within the semi-solid temperature range to trigger selective grain-boundary melting and achieve a globular structure [9].

Recently, SSP has been adapted for additive manufacturing (AM) in the form of thixotropic deposition, also known as semi-solid extrusion-based 3D printing. This technique leverages the thixotropic behavior of partially melted alloys to enable the layer-by-layer fabrication of three-dimensional structures [10]. Unlike powder-based AM methods—which pose safety and handling challenges, particularly with reactive metals—semi-solid extrusion using metallic wires offers a potentially safer, cleaner, and more manageable alternative [10].

The idea of using thixotropic materials for additive manufacturing emerged in the 21st century [11]. Initial efforts focused on selecting suitable materials, improving flowability, controlling processing temperature, and ensuring that the printed structures exhibited the desired microstructure and mechanical properties. It was only within the last decade that the feasibility of thixotropic 3D printing was demonstrated in few pioneering scientific studies [5].

One of the pioneering studies in this domain was conducted by Rice et al. [12], who introduced a rheo-casting method in which the metallic alloy is fully melted and then cooled to a partially solidified state before being deposited onto a moving substrate. In 2002, Finke and Feenstra explored the feasibility of a novel approach based on the Fused Filament Fabrication (FFF) technique [11]. They investigated the complex relationship between microstructure and processing parameters, demonstrating that both the extrusion and deposition processes are strongly influenced by the rheological properties of the semi-solid alloy.

In another study, Mireles et al. examined the application of the FFF technique to low-melting-point metallic alloys, primarily from the Bi-Sn system, for the fabrication of electronic interconnects [13]. Their work successfully demonstrated the deposition of single-layer solder lines of varying thicknesses, including sharp 90° angles and smooth curved geometries.

More recently in 2017, Chen et al. introduced an alternative technique for processing semi-solid alloys, known as Direct Metal Writing. Their method involved controlling

the microstructure of semi-solid alloy slurries to achieve a suitable viscosity range and shear-thinning behavior—key characteristics for enabling stable and precise deposition [14]. To validate the feasibility of their approach, Chen et al. used a binary Bi-Sn alloy and successfully achieved steady-state printing of 3D metallic structures. A notable contribution also comes from Jabbari and Abrinia [15,16], who not only demonstrated the viability of this technique using low-melting point Sn-Pb alloys but also patented their own version of an additive manufacturing apparatus based on semi-solid wire extrusion in 2018 [17].

In 2020, Lima et al. [18] conducted experiments on Mg-Zn alloys, focusing on microstructural evolution and optimizing the formation of a globular structure. Notably, they aimed to induce the globularization of the grains directly during the printing process. This marked a significant advancement in production efficiency, as it reduced the time required for feedstock preparation.

More recently, in 2022 Englert et al. [19] employed an AlSi7Mg alloy for the fabrication of tri-dimensional objects through thixo-printing. This represented a major step forward, as aluminum and its alloys are far more commonly used in industrial applications than Sn-Pb and Mg-Zn alloys. Moreover, to address the challenge of protecting semi-solid aluminum from oxidation due to air exposure, they developed an improved instrumental setup. This included a protective chamber that significantly reduced oxidation and enhanced interlayer adhesion, as well as an induction system capable of reaching higher temperatures more rapidly.

Despite the potential of thixotropic metal AM, several key challenges remain. These include maintaining consistent globularization during printing, preventing oxidation in ambient air, and developing compatible hardware capable of precise temperature control and synchronized motion.

This study provides experimental insight into the feasibility of thixotropic wire extrusion using an Al-Si alloy (EN AW-4043), with a focus on achieving in situ globularization during dynamic processing. Specifically, it demonstrates that a globular microstructure can be obtained by heating cold-worked alloy wires within the semi-solid temperature range for short durations. The proposed system employs an induction-heated nozzle to dynamically replicate these conditions during extrusion, thereby validating the semi-solid extrusion process.

It is important to note that the aim of this study is not to develop a fully integrated 3D printer, but rather to assess whether the required microstructural transformation—globularization—can occur in situ, directly within the heated printing nozzle during deposition. By demonstrating this capability, the approach eliminates the need for pre-cast or pre-globular feedstock and opens new possibilities for applying thixotropic deposition to standard wrought aluminum alloys.

2. Materials and Methods

The EN AW-4043 aluminum alloy was selected for this study due to its relatively low melting temperature and wide solidus–liquidus interval, key prerequisites for enabling semi-solid metal extrusion and deposition (SSMED) in additive manufacturing. To identify the most suitable processing window, thermodynamic simulations were carried out using Thermo-Calc software (version 2023a), employing the TCAL 8 database for aluminum alloys (v8.2, Stockholm, Sweden).

The chemical composition of the EN AW-4043 alloy used in both the experimental trials and thermodynamic simulations was determined using Optical Emission Spectrometry (Q4 TASMAN, Bruker, Billerica, MA, USA) and is presented in Table 1.

Table 1. Chemical composition of the alloy EN AW-4043 alloy (wt%).

Si	Fe	Cu	Mn	Mg	Zn	Ti	Al
4.315	0.138	0.021	0.002	0.002	0.006	0.008	Balance

The alloy was supplied in rod form (Ø 3.2 mm) from Vogelmann Welding© (Bytom, Poland). Cold rolling was applied using a laboratory-scale caliber rolling mill (F.lli Cavallin, Bussero, Milano, Italy) to reduce the rod diameter to 2 mm and 1 mm, corresponding to plastic deformations of 60.2% and 90.2%, respectively.

Furnace heat treatments were performed at 574 °C and 590 °C on both as-received and cold-worked samples, with holding times of 5, 10, and 15 min. These temperatures were selected based on Thermo-Calc results to evaluate the alloy's ability to develop a globular microstructure when heated within or just below the semi-solid temperature range. Following heat treatment, samples were rapidly quenched in water to preserve the resulting microstructure for further analysis by optical and scanning electron microscopy (SEM).

For metallographic characterization, samples were embedded in conductive resin using the EP16 Hitech Europe mounting system (Corsico, Milano, Italy), with the wire axis oriented parallel to the mounting plane. Sample preparation involved sequential grinding with SiC paper (grit P320–P2500), followed by polishing with 3 μm and 1 μm diamond suspensions. Optical microscopy was conducted using a Nikon Eclipse LV150NL (Tokyo, Japan) microscope equipped with a Nikon DS-U3 digital camera and NIS Elements v4.60 software (Tokyo, Japan). High-resolution microstructural analyses were conducted using a Zeiss Sigma 500 FE-SEM (Jena, Germany), equipped with an Oxford Instruments Ultim Max EDS detector and a C-Nano EBSD detector for elemental and crystallographic analysis (Tubney Woods, Abingdon, UK). EBSD post-processing was carried out using AZtecCrystal software (version 3.1, Tubney Woods, Abingdon, UK). To distinguish the Si and Al phases—which both possess face-centered cubic structures with similar lattice parameters—manual phase identification training was performed based on the elemental compositions of primary and eutectic phases. Pixels corresponding to eutectic Si were filtered out from the final EBSD maps, resulting in some unindexed gray regions.

Vickers microhardness measurements were performed on samples polished to a 1 μm finish using a Future Tech FM-810 Micro Vickers hardness tester (Corsico, Milano, Italy), applying a 300 gf load for 15 s. A minimum of five measurements were taken for each condition to determine the mean hardness value.

Following validation of the alloy's suitability for SSMED, a custom extrusion head equipped with an induction heating system was designed, manufactured, and integrated into a laboratory-scale thixo-printing prototype.

Extrusion tests were carried out using the induction-heated printing head powered by a 12 kW generator. The heating element comprised a solenoidal coil made of two turns of 5 mm diameter copper tubing, water-cooled to ensure thermal stability during operation. The coil had an internal diameter of 85 mm, with an axial spacing of 20 mm between the turns. The aluminum alloy wire was mechanically fed at a constant feed rate of 1.25 mm/s, an optimal value chosen to provide sufficient residence time within the heated zone for the desired microstructural transformation to occur.

To optimize the thermal conditions for in situ globularization, thermal profiling of the nozzle was performed. Three thermocouples were strategically positioned at specific points within the nozzle to correlate the temperature experienced by the wire during dynamic flow with the reference temperatures established from furnace tests.

Preliminary deposition trials were conducted by printing onto a quartz substrate placed 10 mm below the nozzle tip. Quartz was chosen to prevent electromagnetic interference with the induction coil.

3. Results and Discussion

3.1. Furnace Thermal Treatments

Thermo-Calc analysis was employed to determine the optimal temperature range for processing the EN AW-4043 aluminum alloy in the semi-solid state. The results revealed an abrupt change in solid fraction within a specific temperature interval. As shown in Figure 1, the alloy exhibits a steep increase in solid fraction between 634 °C and 574 °C, primarily due to the solidification of the primary α-Al phase. Additionally, a sudden increase in solid fraction occurs around 574 °C, corresponding to the solidification of the Al-Si eutectic.

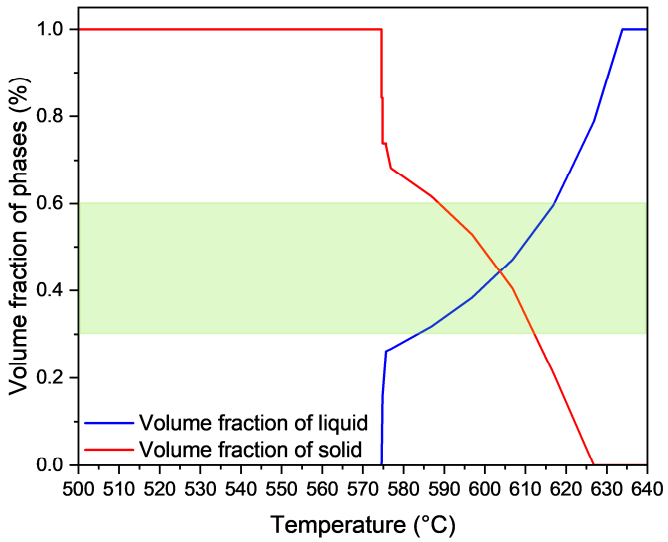

Figure 1. Volume fraction of the two main phases of the EN AW-4043 alloy under equilibrium solidification; the green area represents the optimal range for semi-solid processing, corresponding to 30–60% of the solid fraction.

According to the literature [20], optimal rheological behavior in semi-solid metals is typically achieved with a solid fraction between 0.3 and 0.6. For the EN AW-4043 alloy, this range corresponds to a temperature range between 588 °C and 614 °C, highlighted as the green region in Figure 1. This 26 °C processing window is considered suitable for semi-solid processing, as it allows stable operation without drastic changes in the solid fraction.

To evaluate the feasibility of achieving an in situ globular microstructure during semi-solid extrusion, EN AW-4043 alloy rods (initial diameter 3.2 mm) were cold-rolled to diameters of 2 mm and 1 mm, corresponding to plastic deformations of 60.2% and 90.2%, respectively. Following cold work, the alloy's hardness increased from 40 HV in the as-received condition to 54 ± 6 HV and 58 ± 7 HV, representing a hardness increase of approximately 35% and 45%, respectively. This increase highlights the effect of strain hardening induced by plastic deformation. The microstructures of the as-received and cold-worked rods are shown in Figure 2. All the samples display a similar microstructure composed of an α-Al matrix (light gray) with homogeneously dispersed Si particles (dark gray).

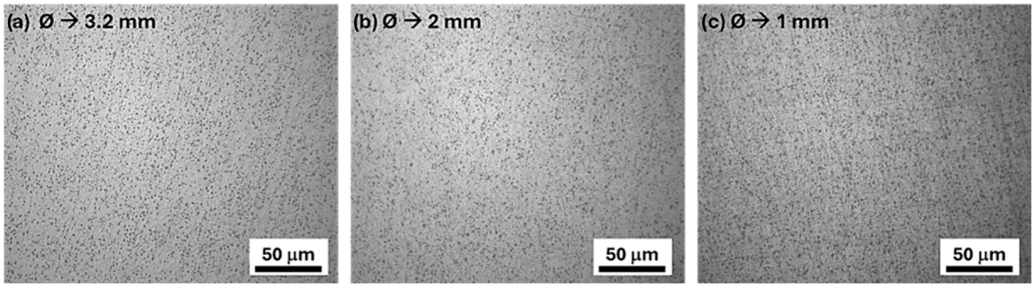

Figure 2. Microstructure of the 3.2 mm as-received rod (**a**) and of the cold-rolled rods with diameters reduced to 2 mm (**b**) and 1 mm (**c**).

Heat treatment is a critical step in obtaining a globular structure after cold working. Based on the Thermo-Calc results, two target temperatures were selected: 574 °C (just below the semi-solid window) and 590 °C (within the semi-solid range), corresponding to solid fractions of 0.73% and 0.58%, respectively. The lower temperature is expected to primarily melt the eutectic fraction, while the higher temperature also induces partial melting of the α-Al phase. To simulate realistic in-nozzle conditions while allowing sufficient time for transformation in the furnace, holding times of 5, 10, and 15 min were adopted.

Heat treating the samples at 574 °C did not produce significant microstructural changes. In contrast, increasing the temperature to 590 °C resulted in the formation of a clearly globular microstructure composed of rounded α-Al grains (light gray) surrounded by a eutectic Al-Si phase (dark gray), as shown in Figure 3. Small eutectic islands were also observed within some α-Al grains, indicating partial entrapment of the liquid phase followed by solidification. Extending the holding time at 590 °C enhanced globularization and promoted moderate grain growth, as confirmed by the data presented in Table 2 and Figure 4.

EBSD analyses of the cold-worked rods (2 mm and 1 mm) prior to heat treatment revealed elongated grains oriented along the rolling direction (Figure 5).

After thermal exposure at 574 °C, signs of recrystallization and eutectic melting were observed, resulting in coarser and more equiaxed grains but with limited globularization due to the short soaking times. In contrast, treatment at 590 °C produced fully developed α-Al globular grains with a more uniform crystallographic orientation.

The hardness of the heat-treated rods decreased to 50 ± 3 HV (60.2% cold work) and 53 ± 5 HV (90.2% cold work) after exposure at 590 °C, compared to their pre-treatment values of 54 ± 6 HV and 58 ± 7 HV, respectively. Although a slight reduction occurred due to partial recrystallization and recovery, the hardness remained well above the as-received level (40 HV), suggesting that the globular microstructure retains improved mechanical properties.

Table 2. Median values of the α-Al Equivalent Circular Diameter (ECD) and roundness for the 2 mm and 1 mm wires heat-treated in a static furnace at 590 °C for different holding times.

	Median of α-Al ECD 2 mm [µm]	**Roundness 2 mm**	**Median of α-Al ECD 1 mm [µm]**	**Roundness 1 mm**
5 min	36 ± 2	0.6	36 ± 6	0.7
10 min	49 ± 2	0.7	50 ± 16	0.7
15 min	53 ± 4	0.8	62 ± 11	0.6

These findings establish the microstructural targets necessary for achieving semi-solid conditions in situ within the induction-heated extrusion head. Although the furnace

holding times may exceed those realistically achievable during wire feeding, adjustments to temperature and feed rate during dynamic processing can be used to compensate for this and replicate the desired microstructural conditions during printing.

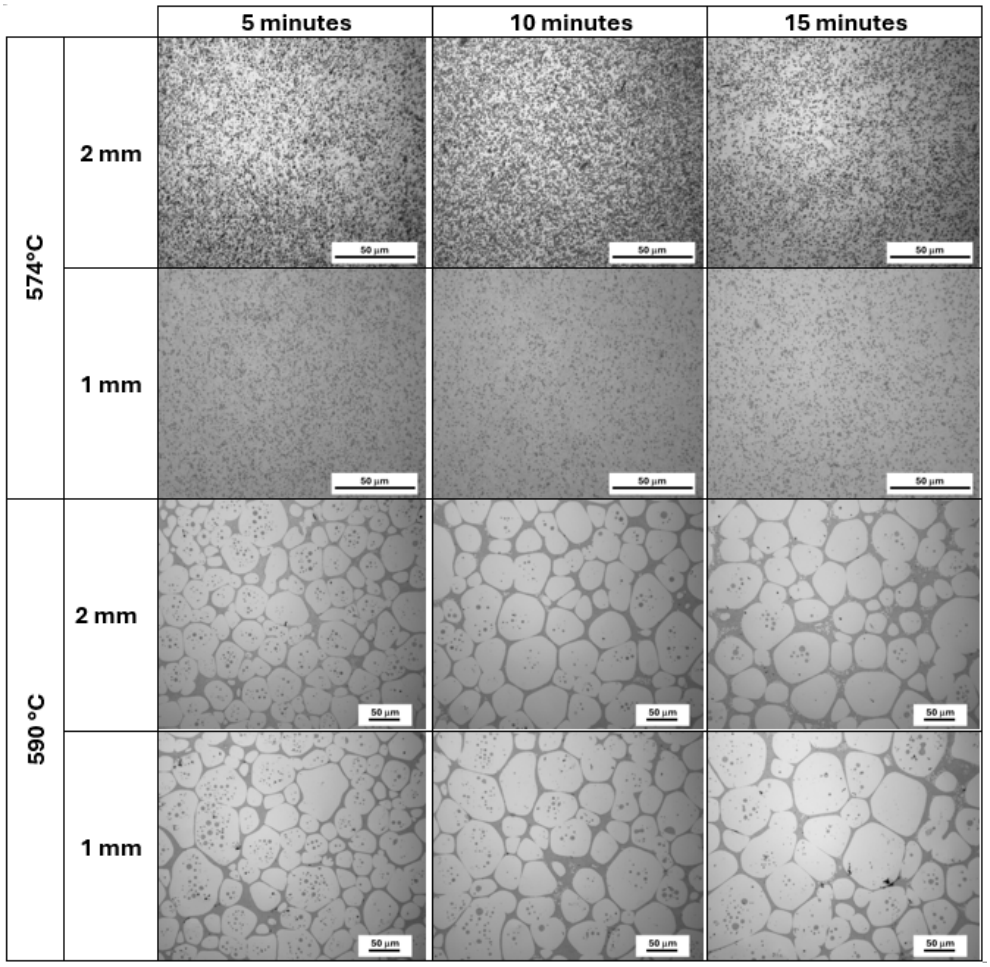

Figure 3. Evolution with treatment time of the microstructural features of the EN AW-4043 rods with different diameters upon thermal treatment at 574 °C and 590 °C.

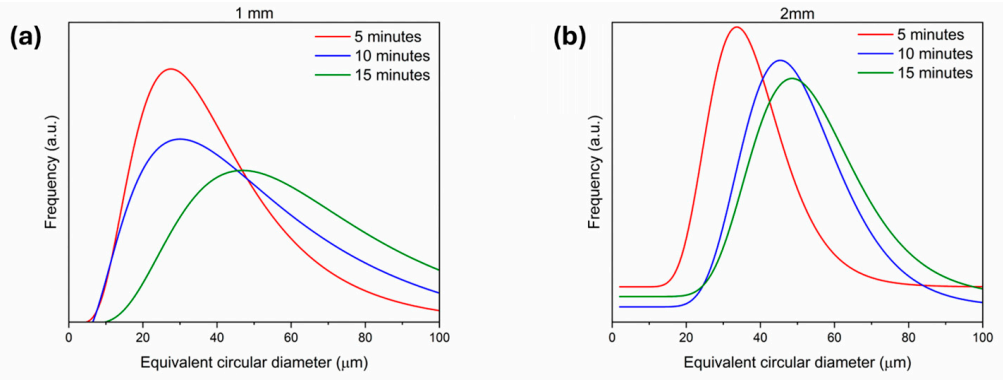

Figure 4. α-Al grain size distribution for wires cold-rolled to 1 mm (**a**) and 2 mm (**b**), after heat treatment in a static furnace at 590 °C for different holding times.

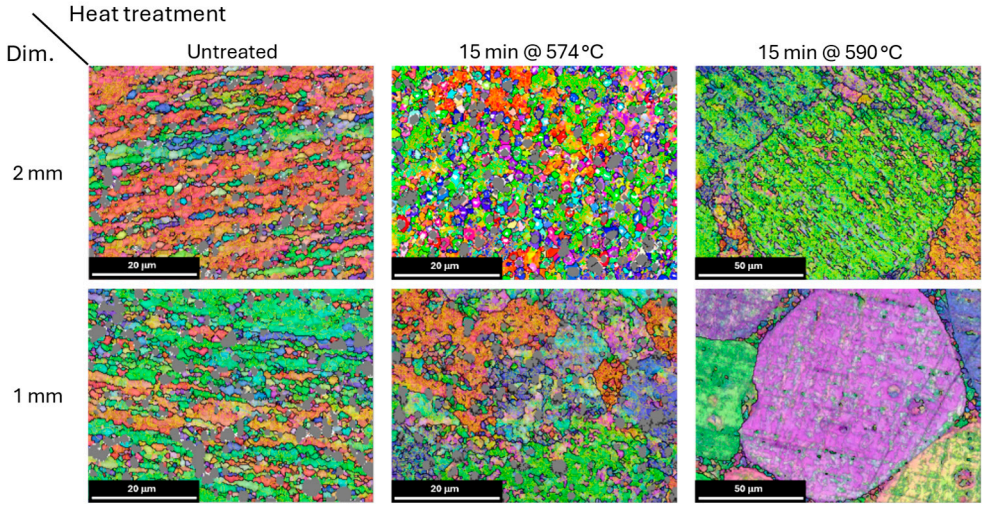

Figure 5. EBSD maps representing the grain evolution of the EN AW-4043 rods with different diameters upon holding for 15 min at 574 °C and 590 °C (rolling direction is horizontal in the images).

3.2. Design of the Nozzle for Thixotropic 3D Printing

The design of the nozzle for the thixotropic 3D printing head is illustrated in Figure 6.

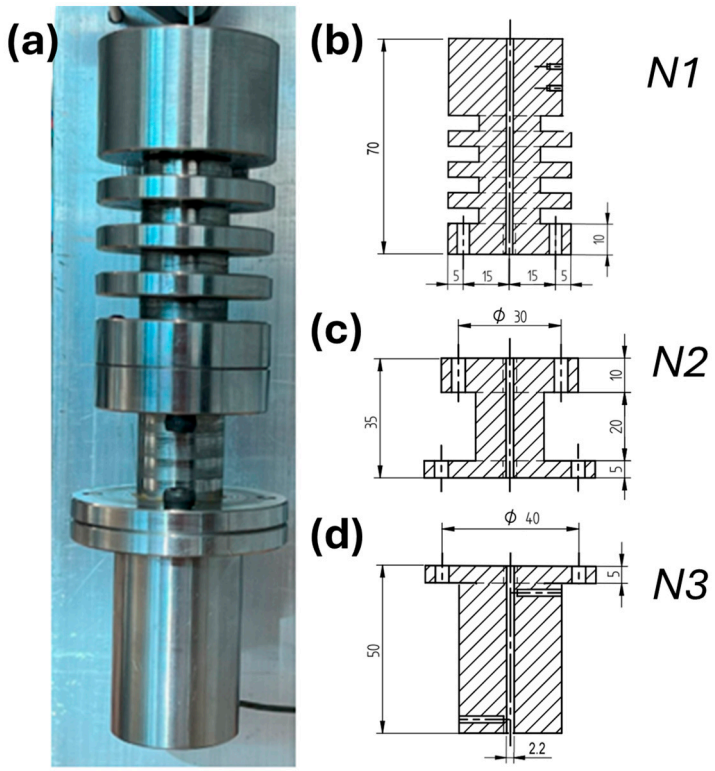

Figure 6. Custom-made printing head for the laboratory-scale thixo-printing system realized in 304 stainless steel (**a**) and technical drawings of the different parts (**b**–**d**).

The component labeled N1 (Figure 6b) corresponds to the upper section of the nozzle, which receives the aluminum wire from the feeding system. This section features a set of cooling fins designed to thermally insulate the incoming wire and protect the feeding mechanism from the heat generated in the lower sections of the nozzle.

Section N2 (Figure 6c) serves as a connecting collar designed to facilitate the assembly and replacement of the lower part of the nozzle. This modularity allows compatibility with various induction coils, which may differ in length or geometry.

Section N3 (Figure 6d) is the lower segment of the nozzle, housing the induction coil and responsible for delivering the semi-solid material onto the build platform. This section is also equipped with lateral holes for thermocouple insertion, enabling real-time temperature monitoring and thermal profiling during the extrusion process.

The entire printing head was fabricated from AISI 304 austenitic stainless steel to ensure high-temperature resistance, structural integrity, and corrosion protection. The nozzle features threaded holes for secure integration with an aluminum support frame and for connection to the wire feeding system.

A complete view of the assembled laboratory-scale thixo-printing setup, including the printing head and all auxiliary systems used for the thixotropic 3D printing of the EN AW-4043 alloy, is presented in Figure 7.

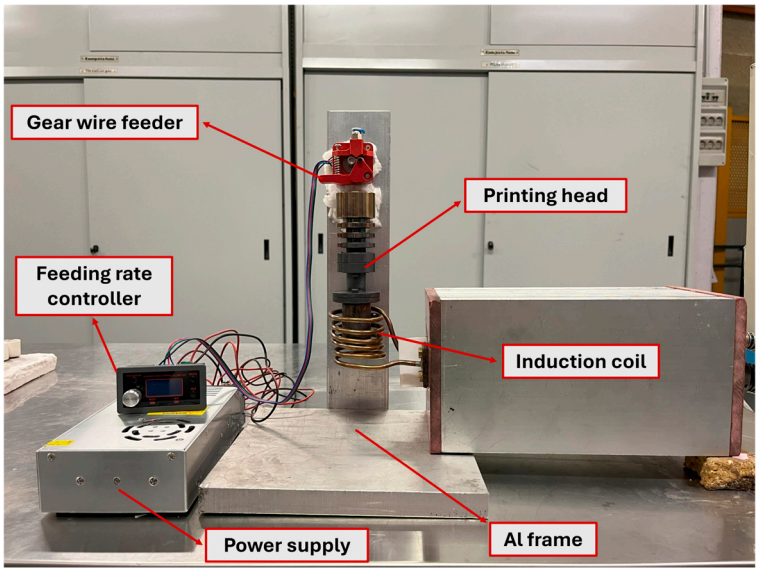

Figure 7. Prototype of the thixotropic 3D printing system.

3.3. Thixotropic 3D Printing Tests

The initial testing phase focused on calibrating the control thermocouples inserted in section N3 with the actual temperature inside the nozzle bore, where the alloy wire is fed. This calibration considered both the shape and position of the induction coil. The goal was to identify a system configuration capable of achieving the target temperature at the nozzle exit while positioning the induction coil to avoid interference with the printing process. As suggested by Jabbari [15], maintaining a nozzle–substrate gap of approximately 1.1 times the nozzle diameter is critical to minimize excessive cooling of the semi-solid alloy—equivalent to only a few millimeters in this case.

A series of tests were conducted targeting wire temperatures of 590 °C, 593 °C, 596 °C, 599 °C, 603 °C, 605 °C, and 610 °C. These temperatures fall within the range identified as suitable for inducing a globular microstructure, based on Thermo-Calc simulations, static heat treatment experiments, and adjustments accounting for the shorter residence times of the moving wire during extrusion.

The primary testing campaign used the 1 mm wire as feedstock. It was estimated that the gear feeder required approximately 2 min to push the wire through the entire length of the nozzle. To ensure reproducibility, multiple samples were extracted from each extrusion trial and immediately quenched in water for microstructural analysis. Each

extrusion condition was repeated several times, yielding consistent results across replicates and confirming the reliability of the observed phenomena.

The results of the optical microscopy analyses are summarized in Figure 8. The microstructure of the wire extruded at 590 °C appeared uniform, showing no evidence of globularization. This likely reflects the shorter exposure time during extrusion compared to the longer durations used in static heat treatments.

The microstructures obtained after extruding the wires at 593 °C and 596 °C were similar to those observed at 590 °C, with the only notable difference being a slight coarsening of the silicon particles. A comparable trend was reported by Ma et al. [21], who observed that silicon particles tend to mature and increase in density following hot extrusion due to the thermodynamic instability of the supersaturated α-Al matrix. Subsequent thermal exposure promotes the precipitation of dissolved Si atoms, resulting in the formation of coarser particles [22].

At 599 °C, initial signs of matrix recrystallization and α-Al grain globularization began to emerge. This transformation is facilitated by the coalescence of Si particles at elevated temperatures, which form a continuous low-melting eutectic network surrounding the evolving globular α-Al grains [19].

At 603 °C and 605 °C, a fully globular microstructure was clearly observed. Over time, Si particles initially dispersed within the α-Al grains migrated toward the grain boundaries, joining the Al-Si eutectic phase. This behavior is driven by Ostwald ripening, a process where atoms diffuse from smaller, energetically less favorable particles to larger ones, thereby reducing the system's overall energy. The high atomic mobility at these temperatures accelerates this phenomenon.

At 610 °C, although globularization remained evident, excessive grain coarsening and irregular grain shapes were observed, indicating that this temperature exceeds the optimal processing range. Therefore, 600 °C was selected as the target temperature for subsequent printing trials.

Printing tests were conducted on quartz substrates to deposit continuous strips of the EN AW-4043 alloy in its semi-solid state.

As shown in Figure 9a, the primary challenge during deposition was poor adhesion between the semi-solid aluminum wire and the quartz substrate, which caused curling of the extruded material. Post-extrusion microstructural analysis (Figure 9b–e) confirmed the successful formation of a globular α-Al microstructure in the initial segments of the wire, validating the effectiveness of the heating strategy. In this region, the average α-Al grain size was smaller than that obtained through static furnace treatment (28 $\pm$ 10 μm), while the roundness remained nearly unchanged. This demonstrates that the in situ heating process effectively promotes grain globularization without compromising morphological uniformity. The measured hardness in this zone was comparable to that of the 90.2% cold-worked samples heat-treated at 590 °C, further supporting the reproducibility and reliability of the in situ treatment approach. However, as extrusion progressed, the microstructure gradually evolved toward features characteristic of lower-temperature treatments. This trend is likely due to progressive thermal losses from exposure to the cooler environment, disrupting the thermal equilibrium needed to maintain the globular structure along the entire length of the wire.

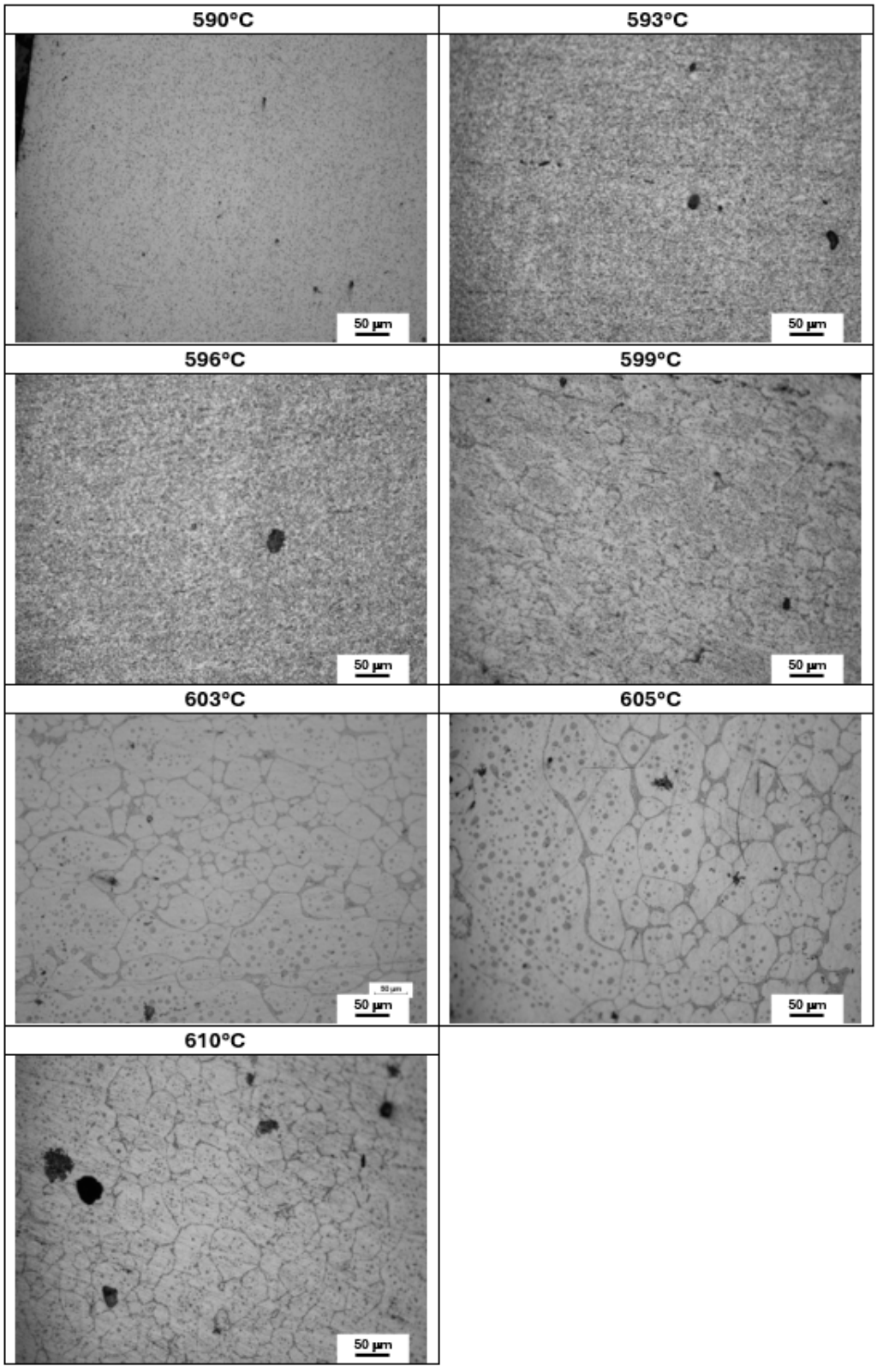

Figure 8. Microstructural features of the wires extruded at different temperatures using the thixotropic 3D printing setup.

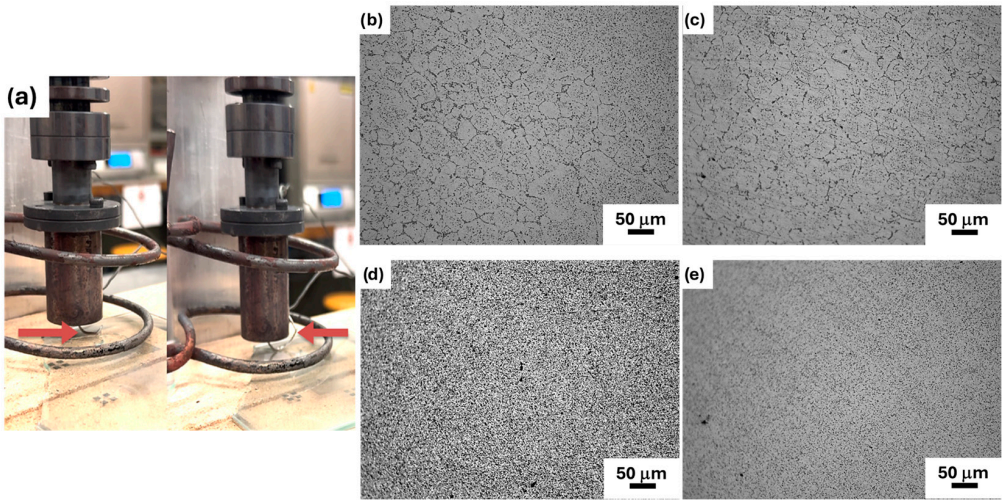

Figure 9. Views of different stages of the thixo-printing extrusion process of the 1 mm EN AW-4043 wire performed at 600 °C using quartz as the substrate material (**a**). Microstructural evolution of the thixo-printed wires moving from the first portion to the last portion of the extruded wire (**b**–**e**).

The poor adhesion observed between the semi-solid aluminum alloy and the quartz substrate is primarily due to the low wettability of aluminum on ceramic surfaces and the substrate's smooth texture. While metallic substrates could improve wetting and adhesion, their strong electromagnetic coupling with the induction coil poses challenges, causing uncontrolled heating and process instability. Quartz and other ceramics, conversely, offer thermal stability and electromagnetic transparency but suffer from inherently poor wetting properties. A potential compromise could involve increasing the substrate's surface roughness and/or coating it with a thin metallic layer that has low inductive coupling. This approach might enhance wetting while maintaining thermal control. Additionally, since surface oxides and contaminants significantly reduce wetting, performing the process in an inert or vacuum environment could further improve interfacial quality. However, implementing such enhancements—including inert gas shielding or a fully automated multi-axis deposition system—would require substantial upgrades to the current laboratory-scale setup. These represent promising directions for future research. Although optimizing the printing head design and processing parameters is beyond the scope of this study, the results presented here mark a significant step forward in thixotropic 3D printing of aluminum alloys. This work has demonstrated the feasibility of depositing EN AW-4043 in a semi-solid state with a globular microstructure directly from commercial cold-drawn wire feedstock—a critical requirement for achieving thixotropic flow behavior.

The globular microstructure was achieved through a carefully calibrated in situ heat treatment, based on the SIMA principle. This method combines severe plastic deformation from cold rolling with precisely controlled induction heating inside the nozzle. The resulting thermo-mechanical synergy promotes partial melting and transforms the microstructure from elongated grains into fine, equiaxed α-Al globules surrounded by the Al-Si eutectic phase.

These findings confirm the viability of semi-solid additive manufacturing with aluminum alloys and establish a foundation for advancing a functional thixotropic 3D printing system capable of precise layer-by-layer deposition with enhanced control over microstructure and material flow.

4. Conclusions

Thermodynamic simulations identified the optimal semi-solid processing window for the EN AW-4043 alloy—corresponding to a solid fraction between 0.3 and 0.6—as lying between 588 °C and 614 °C.

Following the strain-induced melt activation strategy, a globular microstructure was achieved by cold working the alloy wires, followed by thermal treatment that transformed the elongated grains—resulting from cold rolling—into the desired globular α-Al grains surrounded by the eutectic phase.

The effects of heat treatment parameters were evaluated: heating at 590 °C for 5 min successfully globularized wires cold-rolled down to 2 mm and 1 mm diameter, while longer holding times led to grain coarsening.

A prototype thixo-printing system was developed and optimized. The printing head successfully produced the target globular microstructure dynamically during extrusion.

Extrusion tests demonstrated that 600 °C is the minimum effective temperature to induce globularization during continuous wire heating. Temperatures above this, such as 610 °C, resulted in excessive grain coarsening and early signs of melting.

Based on these results, 600 °C was selected as the optimal printing temperature. Printing trials on quartz substrates revealed wire curling caused by poor adhesion and the substrate's smooth surface. However, microstructural analysis confirmed the formation of the globular structure at the initial extrusion stage. As more material accumulated, a transition to a non-globular microstructure was observed, likely due to variations in heat dissipation conditions.

Although further development—such as the integration of shielding gas and a motorized XYZ stage—are necessary to achieve full 3D printing functionality, this study demonstrates the feasibility of producing of a globular microstructure via in situ heating of cold-worked EN AW-4043 aluminum wire, thereby validating the strain-induced melt activation approach for thixotropic metal extrusion.

Author Contributions: Conceptualization, M.V. and S.M.; methodology, S.M.; investigation, S.M.; resources, M.V.; data curation, S.M.; writing—original draft preparation, S.M.; writing—review and editing, M.V.; supervision, M.V. All authors have read and agreed to the published version of the manuscript.

Funding: This research received no external funding.

Data Availability Statement: Data will be made available by the authors upon request.

Conflicts of Interest: The authors declare no conflicts of interest.

Abbreviations

The following abbreviations are used in this manuscript:

SSP	Semi-solid processing
SIMA	Strain-induced melt activation
AM	Additive manufacturing
FFF	Fused filament fabrication
SSMED	Semi-solid metal extrusion and deposition
FE-SEM	Field emission scanning electron microscope
EDS	Energy dispersive x-ray spectroscopy
EBSD	Electron back-scattered diffraction
ECD	Equivalent Circular Diameter

References

1. Flemings, M.C. Behavior of Metal Alloys in the Semisolid State. *Metall. Trans. A* **1991**, *22*, 957–981. [CrossRef]
2. Fan, Z. Semisolid metal processing. *Int. Mater. Rev.* **2002**, *47*, 49–86. [CrossRef]
3. Barnes, H.A. Thixotropy a review. *J. Non-Newton. Fluid Mech.* **1997**, *70*, 1–33. [CrossRef]
4. Kirkwood, D.H. Semisolid Metal Processing. *Int. Mater. Rev.* **1994**, *39*, 173–189. [CrossRef]
5. Fei, Y.; Xu, J.; Yao, D.; Zhou, J. From semisolid metal processing to thixotropic 3D printing of metallic alloys. *Virtual Phys. Prototyp.* **2022**, *17*, 489–507. [CrossRef]
6. Czerwinski, F. Semisolid Processing—Origin of Magnesium Molding. In *Magnesium Injection Molding*; Springer: Boston, MA, USA, 2008; pp. 81–147. [CrossRef]
7. Spencer, D.B.; Mehrabian, R.; Flemings, M.C. Rheological Behavior of Sn-15 Pct Pb in the Crystallization Range. *Metall. Trans.* **1972**, *3*, 1925–1932. [CrossRef]
8. Czerwinski, F. Critical Assessment 32: Controling the melting behaviour of cast structures through solid-state deformation. *Mater. Sci. Technol.* **2019**, *35*, 999–1006. [CrossRef]
9. Zhang, Q.; Li, H.; Han, B.; Huang, K.; Fang, X.; Chen, Z. A distinctive Pb-Sn semi-solid additive manufacturing using wire feeding and extrusion. *J. Manuf. Process.* **2022**, *80*, 247–258. [CrossRef]
10. DebRoy, T.; Wei, H.L.; Zuback, J.S.; Mukherjee, T.; Elmer, J.W.; Milewski, J.O.; Beese, A.M.; Wilson-Heid, A.; De, A.; Zhang, W. Additive manufacturing of metallic components—Process, structure and properties. *Prog. Mater. Sci.* **2018**, *92*, 112–224. [CrossRef]
11. Finke, S.; Feenstra, F.K. Solid freeform fabrication by extrusion and deposition of semi-solid alloys. *J. Mater. Sci.* **2002**, *237*, 3101–3106. [CrossRef]
12. Rice, C.S.; Mendez, P.F.; Brown, S.B. Metal Solid Freeform Fabrication Using Semi-Solid Slurries. *JOM* **2000**, *52*, 31–33. [CrossRef]
13. Mireles, J.; Kim, H.C.; Lee, I.H.; Espalin, D.; Medina, F.; Macdonald, E.; Wicker, R. Development of a fused deposition modeling system for low melting temperature metal alloys. *J. Electron. Packag.* **2013**, *135*, 011008. [CrossRef]
14. Chen, W.; Thornley, L.; Coe, H.G.; Tonneslan, S.J.; Vericella, J.J.; Zhu, C.; Duoss, E.B.; Hunt, R.M.; Wight, M.J.; Apelian, D.; et al. Direct metal writing: Controlling the rheology through microstructure. *Appl. Phys. Lett.* **2017**, *110*, 094104. [CrossRef]
15. Jabbari, A.; Abrinia, K. A metal additive manufacturing method: Semi-solid metal extrusion and deposition. *Int. J. Adv. Manuf. Technol.* **2018**, *94*, 3819–3828. [CrossRef]
16. Jabbari, A.; Abrinia, K. Developing thixo-extrusion process for additive manufacturing of metals in semi-solid state. *J. Manuf. Process.* **2018**, *35*, 664–671. [CrossRef]
17. Jabbari, A.; Abrinia, K. Additive Manufacturing Apparatus Using a Semi-Solid Extrusion of Wire. U.S. Patent 2018/0209194 A1, 11 October 2018.
18. Lima, D.D.; Campo, K.N.; Button, S.T.; Caram, R. 3D thixo-printing: A novel approach for additive manufacturing of biodegradable Mg-Zn alloys. *Mater. Des.* **2020**, *196*, 109161. [CrossRef]
19. Englert, L.; Klumpp, A.; Ausländer, A.; Schulze, V.; Dietrich, S. Semi-solid wire-feed additive manufacturing of AlSi7Mg by direct induction heating. *Addit. Manuf. Lett.* **2022**, *3*, 100067. [CrossRef]
20. Han, Q.; Viswanathan, S. The use of thermodynamic simulation for the selection of hypoeutectic aluminum-silicon alloys for semi-solid metal processing. *Mater. Sci. Eng. A* **2004**, *364*, 48–54. [CrossRef]
21. Ma, P.; Jia, Y.; Prashanth, K.G.; Yu, Z.; Li, C.; Zhao, J.; Yang, S.; Huang, L. Effect of Si content on the microstructure and properties of Al–Si alloys fabricated using hot extrusion. *J. Mater. Res.* **2017**, *32*, 2210–2217. [CrossRef]
22. Alghamdi, F.; Song, X.; Hadadzadeh, A.; Shalchi-Amirkhiz, B.; Mohammadi, M.; Haghshenas, M. Post heat treatment of additive manufactured AlSi10Mg: On silicon morphology, texture and small-scale properties. *Mater. Sci. Eng. A* **2020**, *783*, 139296. [CrossRef]